Comparative study of heat transfer from Nb-Ti and Nb_3Sn coils to He II

Marco La China and Davide Tommasini
CERN, CH-1211 Genève 23, Switzerland
(Received 24 July 2007; revised manuscript received 18 May 2008; published 7 August 2008)

In superconducting magnets, the energy deposited or generated in the coil must be evacuated to prevent temperature rise and consequent transition of the superconductor to the resistive state. The main barrier to heat extraction is represented by the electric insulation wrapped around superconducting cables. In the LHC, insulation improvement is a key point in the development of interaction region magnets and injector chain fast-pulsed magnets for luminosity upgrade; the high heat load of these magnets, in fact, is not compatible with the use of current insulation schemes. We review the standard insulation schemes for Nb-Ti and Nb_3Sn technology from the thermal point of view. We implement, in an analytical model, the strongly nonlinear thermal resistances of the different coil components including the permeability to superfluid helium of Nb-Ti insulations, measured during the LHC main dipole development. We use such a model to compare Nb-Ti and Nb_3Sn technologies by taking into account their specific operating margin in different working conditions. Finally, we propose an insulation scheme to enhance the heat transfer capability of Nb-Ti coils.

DOI: 10.1103/PhysRevSTAB.11.082401 PACS numbers: 84.71.Ba

I. INTRODUCTION

Heat management is a fundamental aspect of superconducting (SC) magnet design in the presence of substantial heat loads, because coil temperature shall be kept below the transition value determined by operating field and current density.

Heat loads of accelerator superconducting magnets vary considerably depending on magnet type and function; heat in the coil can be either deposited by beam particles or generated inside the magnet as AC losses.

Indicative values of deposited and generated heats are given in Table I in which the LHC main arc dipole is given as comparison.

The main barrier to heat extraction from the coil is represented by electric insulation wrapped around superconducting cables.

The two options for superconducting accelerators magnets, the promising Nb_3Sn and the well-established Nb-Ti, present coexisting aspects that must be taken into account when comparing their heat transfer to superfluid helium.

On one hand, Nb_3Sn has a fairly high critical temperature (~ 18 K) and Nb_3Sn coils are usually impregnated with resin. In fact, coil impregnation is needed in the first place to improve mechanical and electrical properties of the cable insulation after coil heat treatment (reaction) and perform the coil geometry. In addition the impregnation helps also to protect the brittle Nb_3Sn cable.

Coil impregnation represents a drawback in terms of heat extraction capacity as it prevents the direct contact between superconducting cable and superfluid helium.

On the other hand, Nb-Ti has a critical temperature (~ 9 K) much lower than Nb_3Sn. In terms of heat extraction capacity, the consequently small temperature margin is a drawback as it limits the maximum heat that can be drained out of the coil. However, the permeability to helium of Nb-Ti insulation provides a good heat transfer potential.

In this paper we first describe the typical insulation schemes for Nb-Ti and Nb_3Sn (Sec. II). We then focus on the thermal properties of the different components to evaluate the overall heat transfer (Sec. III). We analyze two different operating scenarios to estimate the maximum heat transfer achievable by each technology (Sec. IV). We propose a way to enhance heat transfer across Nb-Ti all-polyimide insulation (Sec. V) and we report the first experimental results (Sec. VI). We summarize and analyze the operative parameters that influence the heat transfer in operative conditions (Sec. VII) and we conclude with some remarks (Sec. VIII).

II. TYPICAL INSULATION SCHEMES FOR ACCELERATOR SC MAGNETS

The design of the electrical insulation of a superconducting magnet depends on several competing factors. In fact, in addition to fulfilling dielectric requirements, the insu-

TABLE I. Heat loads on different types of SC magnets.

Beam induced heat deposition [W/m]	
LHC main arc dipole [1]	LHC IR quadrupole [2]
0.06	7
Heat generation [W/m]	
LHC main arc dipole [1]	GSI fast cycling dipole (SIS 300) [3]
0.4	13

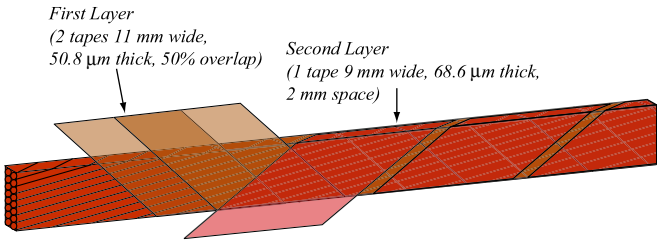

FIG. 1. (Color) State-of-the-art Nb-Ti insulation (LHC type).

lation must possess mechanical strength to withstand the strong compression of the coil and must preserve ductility at cryogenic temperature, must provide cohesion between coils turns to allow coil handling during magnet assembly, must be radiation resistant, and must be able to accommodate thickness variation of the various coil components to facilitate a constant coil size. Finally, it should feature a moderate thermal shrinkage and adequate heat conductivity. All of the above tasks have to be accomplished with a minimum thickness (in the order of 0.1–0.2 mm) to maximize the bare/insulated conductor aspect ratio.

State-of-the-art Nb-Ti insulation, developed for the LHC magnets [1] and shown in Fig. 1, consists of polyimide tapes arranged in layers helically wound around the cable.

The first, inner, layer has the function to dielectrically isolate adjacent turns. The interturn voltage that arises in the case of a quench is around 100 V and the current can make its way across the insulation in correspondence of material defects (punch through), or along the insulation surface. To reduce the punch-through risk and to provide a sufficiently long surface path, the first layer is composed by two 50% overlapped tapes.

The second, outer, layer is intended to protect the first layer during coil winding, magnet assembly, and operation. It must also provide the cohesion between coil turns and must create gaps for helium to reach the inner layer. The second layer consists therefore of a single and thicker polyimide tape with, on the outer face, a thin coat of polyimide adhesive activated by heat treatment. The second layer is wound, with spacing, in the opposite direction with respect to the inner one.

This all-polyimide, two layers solution is the result of a continuous evolution started in the early 1970s for the ISR [4], passing through SSC [5], HERA [6], RHIC [7], and LHC [1].

On top of the features requested by Nb-Ti, Nb_3Sn coils demand to the insulation much more than simple cohesion between turns. An authentic structural envelope is in fact needed to provide mechanical properties to the coil and protect the brittle Nb_3Sn compound. The desired coil rigidity and robustness is commonly achieved through vacuum impregnation with epoxy resin [8]. In case of coil manufactured with the most common *wind and react* technique, the reaction to form the Nb_3Sn compound is accomplished after coil winding. This means that the insulation must withstand temperatures in the range of 650–700°C without downgrading the mechanical properties. Typical Nb_3Sn insulation associated with the *wind and react* technique is composed of a mineral fiber cloth that is wrapped around the cable before winding and thermal treatment: after the thermal treatment the cable is vacuum impregnated with epoxy resin. The fiber cloth has different purposes: it helps in controlling interturn spaces and thus final coil size; it facilitates an even distribution of resin and reduces crack propagations [9].

At this stage of Nb_3Sn technology development, the best solution has not been defined yet and different options are being considered for the fiber cloth. Alternatives are represented by glass fiber tapes or sleeves (by far the most used and practical), mica-glass and glass fiber [10], and quartz fiber. Innovative insulation schemes rely on the use of ceramic/inorganic [11] or all ceramic [12] materials.

III. HEAT TRANSFER THROUGH INSULATIONS

From the heat transfer point of view, out of all the differences between Nb-Ti and Nb_3Sn insulations highlighted in the previous section, fundamental is the impregnation with resin. In vacuum-impregnated coils, in fact, the presence of resin prevents any direct contact between helium and the strands, whereas nonimpregnated coils are permeable to helium.

A schematic representation of Nb-Ti and Nb_3Sn coils, immersed in a superfluid helium bath, is given in Figs. 2 and 3.

In the Nb-Ti case, insulation permeability allows helium to enter and fill meanders between strands forming an internal bath; such an internal bath is connected to the external bath through a network of microchannels between insulation wraps. Heat from the strands to the external bath can thus follow two parallel paths: one formed by helium channels (superfluid conduction path); the other by solid conduction through insulation material. In Fig. 2 we show a representation of the two parallel paths in terms of equivalent thermal resistances. We use such a schematization to model heat transfer across Nb-Ti insulation under the following assumptions: (i) longitudinal heat transfer is negligible; (ii) heat is evacuated through the cable small face; (iii) channel network can be treated as a single channel with equivalent cross section; (iv) strand, internal bath, and external bath are isothermal; (v) parallel paths (superfluid and solid conduction) are decoupled; (vi) thermal boundary resistance at the strand-insulation interface is negligible [13].

Thanks to the very high thermal conductivity of helium, superfluid conduction path is characterized by very low thermal impedance. However, heat transport through superfluid helium channels is limited by the lambda transition (He II turns into He I) at the channel inlet [14]: the very poor thermal conductivity of He I causes in fact a drastic reduction of heat transfer through the channel that is thus considered saturated.

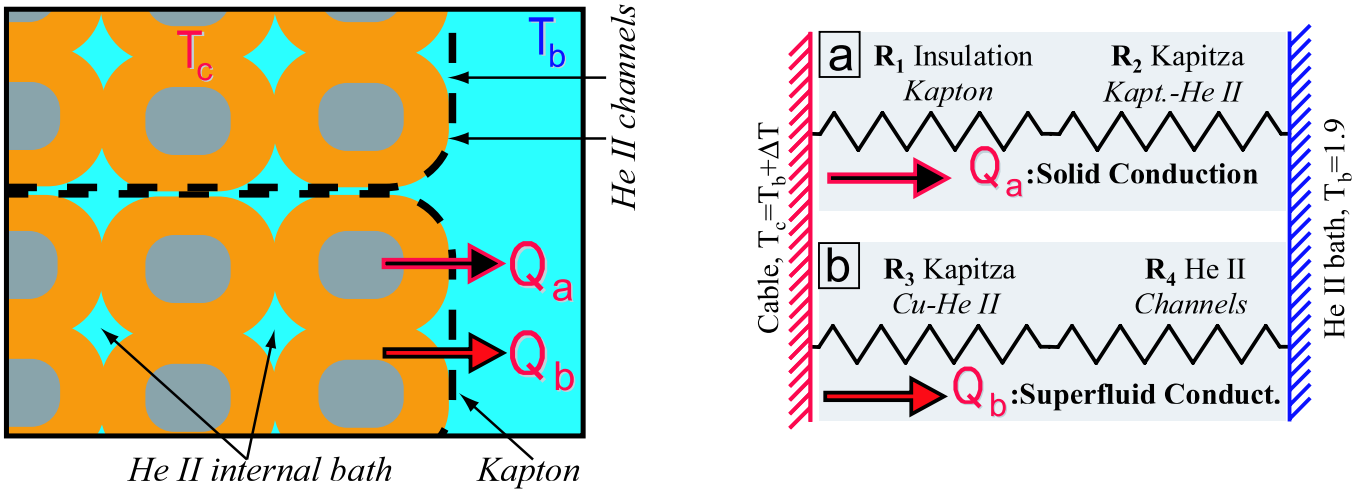

FIG. 2. (Color) Schematization of heat transfer path through *porous* insulation.

Thermal impedance and saturation level depend on channel geometries (cross section, length) and bath temperature [15].

In Nb_3Sn coils the only thermal path available is through the insulation material. In terms of equivalent thermal resistance it can be schematized as shown in Fig. 3. The underlying assumptions are: (i) longitudinal heat transfer is negligible; (ii) heat is evacuated through the cable small face; (iii) thermal boundary resistance at the strand-epoxy interface is negligible [13]; (iv) strand and external bath are isothermal.

In an impregnated coil, heat transfer depends mainly on the thermal conductivity of the fiberglass plus resin system. In this case obviously, heat transfer is not limited by channel saturation.

In the Nb-Ti case, the complex topology of porous insulation requires, in principle, experimental evaluations of the heat transfer achievable in operating conditions. Experimental data can be found in the literature [16,17] and, even if they cannot be directly compared between each other, being based on different experimental setup, they show the remarkable efficiency of the porous insulation in the small temperature increase.

As an example we report data published by Meuris [17] during the development of the LHC main dipole insulation. Heat transfer across insulation was evaluated by measuring the temperature rise of a solid cable mock-up made of steel, heated by the joule effect, immersed in a superfluid helium bath at 1.8 K, and insulated using different insulation schemes.

In Fig. 4 we report mock-up temperature rise versus heat flux for two types of all-polyimide insulation with two distinct levels of permeability to helium: SSC dipole type and LHC dipole type. The SSC dipole insulation scheme was designed to operate in supercritical helium at 4.2 K disregarding permeability criteria whereas LHC dipole insulation is permeable to helium thanks to the tape spacing in the outer layer.

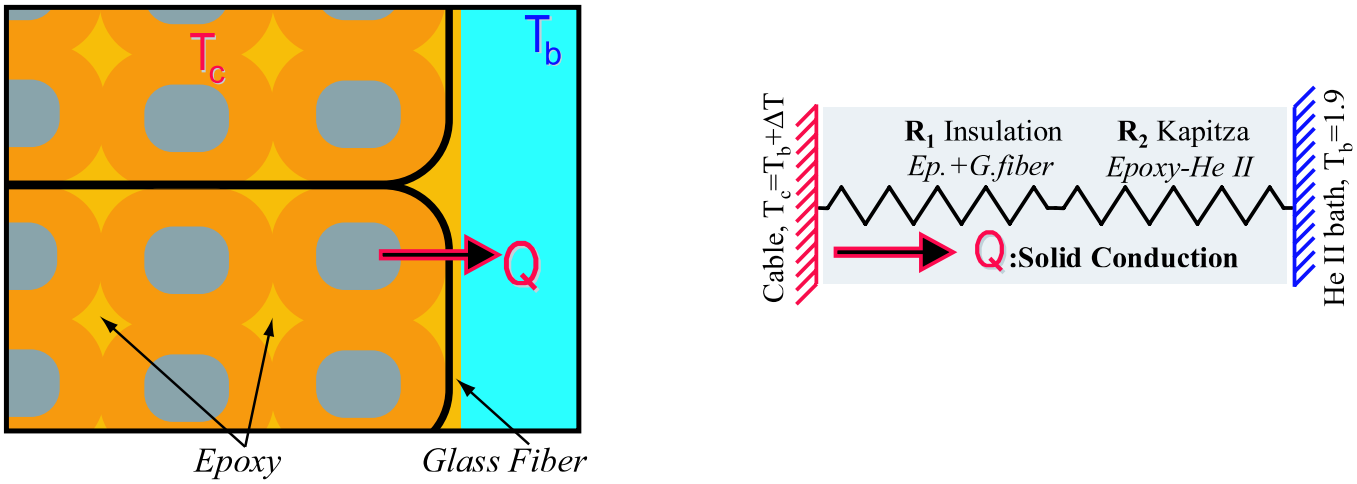

FIG. 3. (Color) Schematization of heat transfer path through *nonporous* insulation.

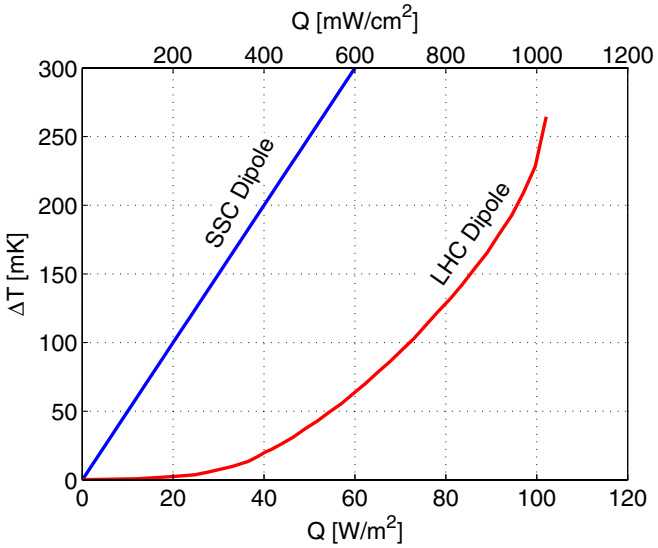

FIG. 4. (Color) Heat transfer curves at $T = 1.8$ K measured by Meuris during LHC main dipole insulation development.

The small permeability of SSC dipole type insulation is remarked by the linear temperature-heat relation featured by the corresponding curve; its constant slope is in fact related to conduction through solid. The LHC curve is strongly nonlinear: the temperature rise is very small for small heat loads and grows fast for higher loads. This means that until temperature increase is small the heat is efficiently transferred through helium channels because of their low impedance. For greater heat loads, channel impedances increase, heat is transferred by conduction through superfluid and through bulk solid but total heat transfer is smaller than before and mock-up temperature increases. Superfluid conduction stops when internal bath reaches lambda transition temperature causing channel saturations; beyond this point heat transfer is dominated by the solid poor thermal conduction. For example, a temperature increase of 10 mK permits the evacuation of 34 W/m^2 for Nb-Ti versus only 2 W/m^2 for SSC.

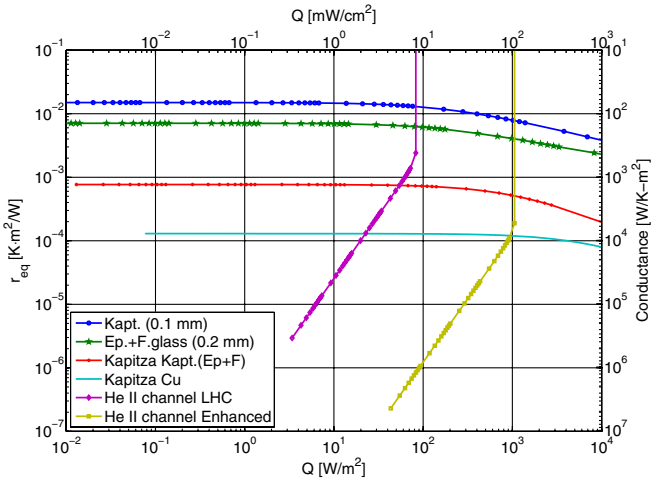

FIG. 5. (Color) Equivalent thermal resistances of insulation components in a 1.9 K helium bath.

To compare the weight, from a thermal point of view, of the different coil components with typical dimensions, we plot, in Fig. 5, the equivalent thermal resistances versus heat flux in a 1.9 K isothermal bath of helium. Conductivity of polyimide (Kaprton) has been measured by Lawrence [18], conductivity of epoxy-impregnated fiberglass has been determined according to experiments reported in [19], boundary resistance at the Cu-He II interface is taken from [20], and at the polyimide-He II interface from [21].

The resistance through the bulk material is computed considering an insulation thickness of 0.1 mm for polyimide and of 0.2 mm for the epoxy + fiberglass composite. Kapitza resistance at the polyimide-He II interface has been considered valid also for epoxy. The resistance of helium channels is given for two different levels of permeability, corresponding to the LHC type insulation and to an enhanced insulation scheme described later (Sec. V).

It is clear how bulk resistance is the most limiting factor for heat transfer and polyimide is less conductive than epoxy-impregnated fiberglass. Helium channels offer a very small thermal resistance that grows fast with heat flux until saturation is reached.

IV. OPERATIVE COMPARISON

To compare Nb-Ti with Nb_3Sn, it is necessary to combine the thermal properties of the insulation with the superconducting properties of the cable.

Conductor properties can be conveniently visualized in a temperature-field-current space as shown in Fig. 6. In such a 3D space, critical values of temperature, field, and current form the critical surface that separates the superconducting region (below the surface) and the normal conducting one (above the surface). Nb_3Sn, having a critical surface more extended than Nb-Ti, offers advantageous superconducting properties, i.e., higher critical current density, field, and temperature.

We consider Nb-Ti and Nb_3Sn insulated coils with a nonsuperconductor to superconductor ratio of 1.5 and 1.0, respectively, immersed in an isothermal helium bath at $T_b = 1.9$ K. We impose homogenous field and current density in each coil to obtain the corresponding transition temperatures. Heat driven by the temperature difference between each coil at transition temperature T_c, and the bath at T_b, represents the maximum heat drainable from the coil. To by-pass geometrical dimensions of the coil, we consider heat flux (heat per unit area in mW/cm^2).

We simulate operating conditions according to two different scenarios: in the first case magnetic field and current density are the same for both the coils, in the second we apply field and current specific for each technology, corresponding to proposals for the upgrade of LHC interaction region magnets [22].

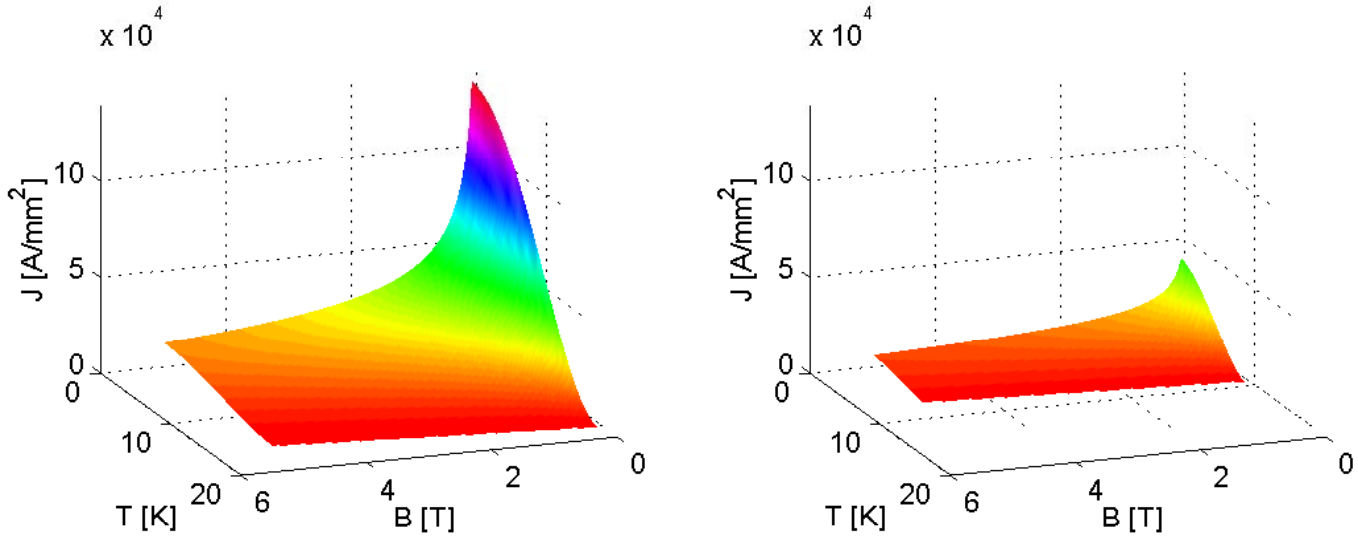

FIG. 6. (Color) Critical surfaces in B, T, J space for Nb_3Sn (left) and Nb-Ti (right).

A. Same operating conditions

It must be primarily pointed out that this first case does not represent typical operating conditions considered for Nb_3Sn. Feeding a Nb_3Sn coil with the same current density as Nb-Ti means, in fact, to use only a small fraction of the available current density; however, the advantage is that coil temperature can increase more and a larger amount of heat can be evacuated. The great difference between temperature rise available to Nb_3Sn and Nb-Ti coil in a 9 T field is visible in Fig. 7. With an overall current density (i.e. the current over the insulated cable cross-section area) of $\sim$800 A/mm^2, at a field of 9 T, the temperature margin available to Nb_3Sn is about 15 times the one of Nb-Ti.

The combination of heat transfer curves and temperature margin curves gives the maximum heat that can be extracted from the coil as plotted, versus the overall current density J_{ov}, in Fig. 8.

For Nb-Ti, we take into account three insulations with different levels of permeability. Two of them are the ones presented in Sec. III (SSC and LHC) whereas the third is the enhanced insulation presented in Sec. V. We also plot the heat transfer in the case of insulation with infinite permeability; this is an asymptotic limit computed by taking into account a cylindrical conductor immersed in a large helium bath.

For Nb_3Sn, we consider 0.2 mm thick epoxy + fiberglass insulation [19].

For an overall current density of around 800 A/mm^2, heat transfer from Nb_3Sn is around 20 times larger than Nb-Ti with nonpermeable insulation (SSC type). Such a

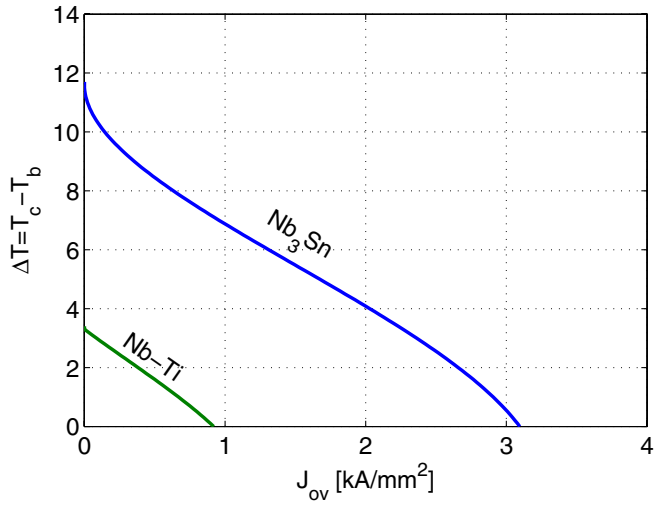

FIG. 7. (Color) Temperature margin versus overall critical current density for Nb-Ti and Nb_3Sn in a 9 T field.

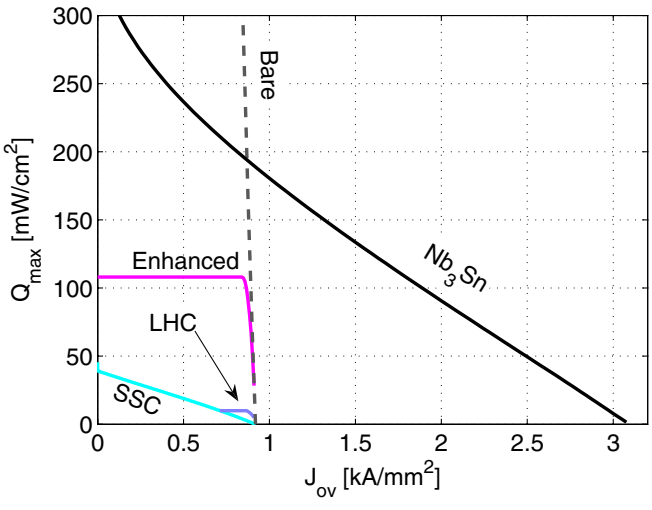

FIG. 8. (Color) Maximum heat flux from Nb-Ti (with insulation: LHC, SSC, enhanced; and without insulation: bare) and Nb_3Sn coils versus overall current density at a magnetic field of 9 T.

big gap between heat transfers through Nb-Ti and Nb_3Sn nonpermeable insulations reflects the difference between temperature margins shown in Fig. 7. In nonpermeable insulations, in fact, the maximum drainable heat is directly related to temperature margin. In permeable insulations, instead, a relatively big heat transfer can be reached with small temperature margin, as revealed by the steep initial slope of the permeable insulation curves (LHC and enhanced). Such a favorable situation terminates with the saturation of helium channels indicated by slope flattening. Then, as the only mechanism left is solid conduction, the only way to increase heat transfer is a drastic increase of conductor temperature; such a temperature rise is attainable through reduction of current density. This situation corresponds to the intersection of the flat part of the LHC insulation curve with the SSC curve at $J_{ov} \sim 0.75\ \mathrm{kA/mm^2}$; at lower J_{ov} the two curves are coincident.

This first comparison shows that sacrificing Nb_3Sn current density in favor of temperature margin can provide very good heat transfer capacity: more than 1 order of magnitude bigger than Nb-Ti.

B. Specific operating conditions

In the second scenario, we compare two alternatives for the upgrade of LHC interaction region quadrupoles described in [22]. In this case Nb_3Sn properties are exploited so that magnetic field and overall current density are, respectively, 50% and 56% higher than in Nb-Ti coil. In Fig. 9 we plot maximum heat transfer versus operative over critical current density ratio.

The Nb_3Sn advantage is drastically reduced with respect to the previous case; current density is now closer to its critical value and the available temperature margin is consequently smaller. In realistic working conditions, current density is kept around 80% of the critical value for stability purpose; from the plot it can be seen that, at this working point, the Nb_3Sn advantage on Nb-Ti is reduced to 3 times. In proximity of critical current density ($J/J_c > 0.95$), where temperature margin is very small, Nb-Ti can even evacuate more heat than Nb_3Sn. The actual Nb-Ti limitation is due to the early saturation of helium channels that reflects limited permeability of insulation. The bare cable asymptotic limit shows, however, that permeability of Nb-Ti insulation can be greatly improved: a possible way to increase the size of helium channels is outlined in the next section.

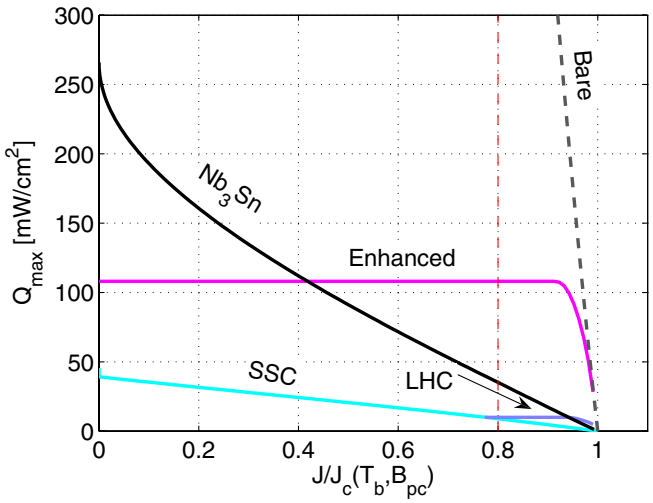

FIG. 9. (Color) Maximum heat flux from Nb-Ti (with insulation: LHC, SSC, enhanced; and without insulation: bare) and Nb_3Sn coils versus operative over critical current density ratio. Comparison for specific operating conditions, Nb-Ti: 9 T; Nb_3Sn: 13.5 T.

V. ENHANCED INSULATION DETAILS

In state-of-the-art insulation schemes for Nb-Ti, the main limitation to heat transfer is due to the overlapped wrapping of the tapes in the first layer. As shown in Fig. 1 in fact, the tapes are directly wrapped one on top of the other leaving in principle no space for cooling channels. However, the first layer always features a certain degree of permeability because helium, thanks to its very low viscosity, can filter between the tapes.

The second layer is wound with spacing to form channels to let helium easily reach the first layer; a second layer with overlap in fact would provide practically helium-tight insulation (SSC type). Yet, the efficiency of spacing in the second layer can be reduced or canceled by other factors: for example, epoxy-impregnated fiberglass tape lets the epoxy flow out during heat treatment, filling up the channels of the second layer [23], contrarily to polyimide glue which does not flow. However, if polyimide glue is present on the internal side of the second layer (to bond first and second layer), it seals the outlets of the first layer channels and permeability is greatly reduced [24].

In fact the studies described in [24] were related to the insulation design similar to the LHC one described in this paper. This insulation had 2 mm gap (channels) in the outer wrap (or second layer) introduced in order to increase the cable wet perimeter. The results of this study clearly indicated that those channels were blocked during coil curing at high temperature and pressure.

In our study we observed that, when no polyimide glue or epoxy accidentally obstructs the channels (described in [24]), the effect of vertical compression on permeability is remarkable only between 0 and 10 MPa. Increasing the compression beyond 10 MPa, in fact, does not change anymore channel size noticeably as the polyimide tape can hardly be squeezed any further.

The baseline concept to enhance insulation permeability is to create channels connecting internal and external helium baths. In our scheme, the two overlapped tapes, originally belonging to the first layer, are split and separated by a series of polyimide strips wound counterwise (Fig. 10).

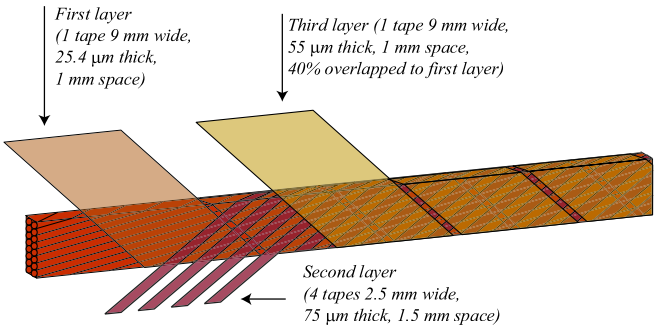

FIG. 10. (Color) Enhanced insulation scheme. Overlap is present between the first and the third layer.

In such a configuration three distinct layers, all wound with spacing, can be identified. The overlap needed to provide a sufficiently long surface path, and to ensure protection against punch-through defects, exists between tapes of the first and third layer (''detached overlap''). The third layer tape, thicker and coated with adhesive on the external side, provides mechanical protection, dielectric protection, and cohesion between turns. Characteristics of state-of-the-art and enhanced insulation can be compared in Tables II and III.

A preliminary estimation of the heat transfer achievable with such an insulation scheme is given in Figs. 8 and 9. It is based on the assumption of a fully developed Gorter-Mellink [25] regime in the channels; the effect of coil compression is introduced in the model as a reduction of channel dimensions.

VI. FIRST EXPERIMENTAL RESULTS

A program of tests has been conceived to progressively validate all the different aspects of the enhanced insulation design. We report here the first part of the experimental program in which we checked the manufacture feasibility of enhanced and standard schemes, and we analyzed the effect of vertical compression on enhanced insulation porosity.

Manual wrapping of new insulation was performed using standard polyimide tapes. According to past experiences no specific issues are expected for the wrapping process automation.

The development of a newly conceived porosity meter device allowed us to compare different insulation schemes applied to Rutherford cables. Cables, of LHC main dipole inner layer type, were arranged in 6 units-stacks and subjected to a vertical compression ranging from 10 to 50 MPa.

The porosity meter uses air at ambient temperature instead of superfluid helium: in this way the experimental setup complexity is drastically reduced. The baseline concept is that both air mass flow and helium heat flow increase with channel cross areas.

Given the strong simplifications inherent to the air-helium analogy and the limited precision of the sensors used, we limit the scope of this experience to a comparative analysis of insulation porosities and to the verification that the new insulation scheme preserves its enhanced porosity under heavy vertical compression.

The porosity meter is a mould designed to force a flow through a 12 cm long cable stack, shown in Fig. 11, along two alternative paths: longitudinal and radial. In the longitudinal path, air crosses the cable stack from end to end (inlet A, outlet C, Fig. 11), without passing through the insulation.

In the radial path, air enters the stack from one end and exits laterally, at half way, thus crossing the insulation (inlet A, outlet B, Fig. 11). In the schematization of the experimental setup, shown in Fig. 12, the porosity of the insulated stack is concentrated in three lumped flow restrictions: R_a R_b, and R_c.

Restrictions R_a and R_c describe the longitudinal porosity of one-half of the cable, each; R_b describes the porosity of the insulation. The longitudinal flow path goes from inlet A to outlet C that is through R_a and R_c; the radial flow path goes from inlet A to outlet B that is through R_a and R_b. Insulation porosity R_b can be thus estimated from the comparison between radial and longitudinal flows.

For each tested insulation we measured the air mass flow along longitudinal and radial paths induced by inlet pressures ranging from 1.2 to 5.0 bar with the outlet at atmospheric pressure (1 bar).

TABLE II. Layer topologies in LHC and enhanced insulation schemes.

	1st layer	2nd layer	3rd layer
State-of-the-art	2 tapes with overlap	1 tape with spacing	
Enhanced	1 tape with spacing	4 tapes with spacing	1 tape with spacing

TABLE III. Specific function of each layer in LHC and enhanced insulation schemes.

	Dielectric protection	Mechanical protection and interturn cohesion	Helium channels
State-of-the-art	1st	2nd	2nd
Enhanced	1st and 3rd (detached overlap)	3rd	1st, 2nd, and 3rd

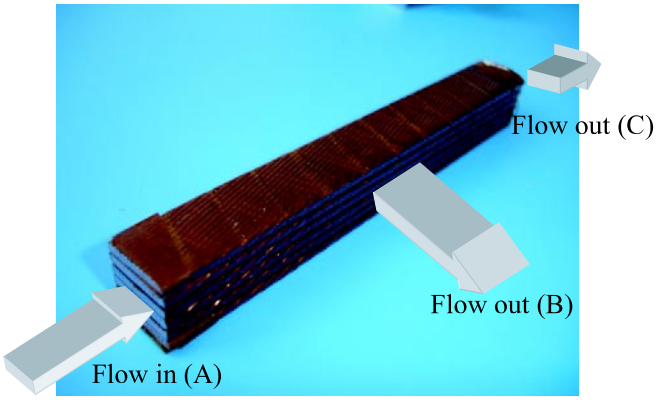

FIG. 11. (Color) Cured stack of insulated cables with radial flow path shown: air enters longitudinally and exits laterally after having crossed insulation wraps.

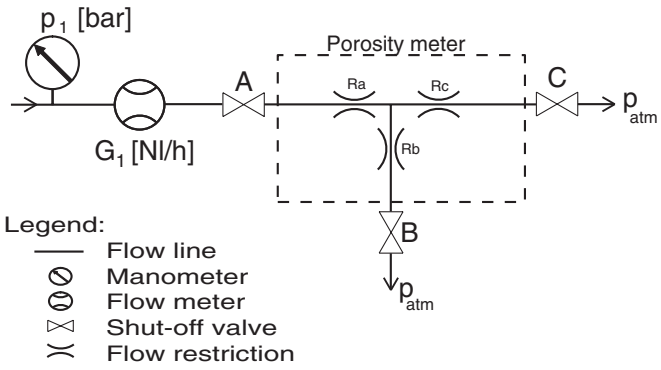

FIG. 12. Equivalent lumped system of test setup.

In Fig. 13 we plot the measured air mass flows versus relative pressure, that is the difference between inlet and outlet pressure.

The three curves refer to the radial flow across a stack of cable with no insulation, LHC insulation, and enhanced insulation; all the stacks are vertically compressed at 10 MPa. The slope of each curve is a direct index of porosity to air: enhanced insulation shows a degree of porosity at least 1 order of magnitude bigger than LHC insulation and one smaller than the bare cable.

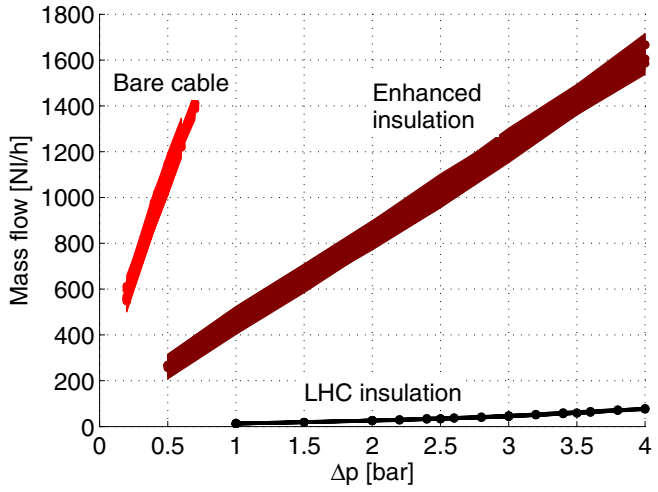

FIG. 13. (Color) Radial flow in cables with no insulation, LHC and enhanced insulations; vertical compression of 10 MPa.

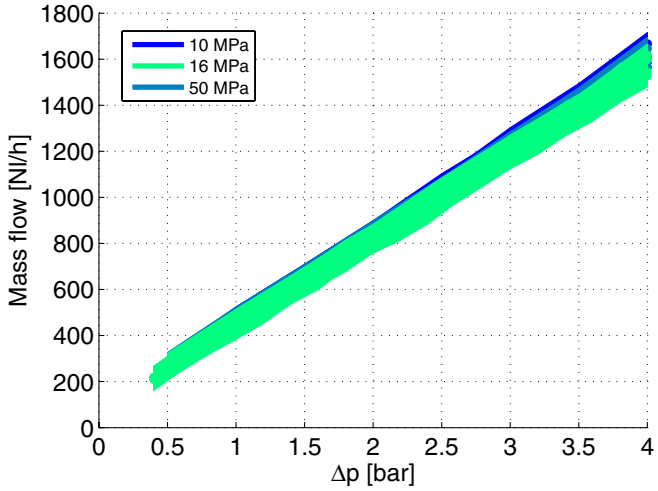

FIG. 14. (Color) Radial flow in cables with enhanced insulation. Vertical compression of 10, 16, and 50 MPa.

In Fig. 14 we show the influence of vertical compression on the new insulation scheme.

The three practically identical curves refer to radial porosity under 10, 16, and 50 MPa. It can be seen that the great porosity measured at 10 MPa is confirmed at 16 and at 50 MPa meaning that the network of channels between insulation wraps is still effective.

In the second part of the experimental program we will verify the dielectric insulation, the resistance to small radius bends, and the actual heat transfer in pressurized superfluid helium.

VII. ANALYSIS OF OPERATIVE PARAMETERS

In this section we analyze the operative parameters that determine the maximum heat transfer in the different scenarios.

The Q-labeled column of Table IV provides the amount of heat drainable across a unitary area of coil surface directly exposed to helium bath as, for example, the inner and the outer radius surface of a $\cos\theta$ dipole coil (Fig. 15). We consider three different insulations for Nb-Ti (SSC type, LHC type, and enhanced) and two operating scenarios for Nb_3Sn, labeled "As Nb-Ti" and "Specific".

In the "Specific" scenario Nb_3Sn is used at 85% of its critical current density at 1.9 K, as shown in the 5th row of Table IV. In this case the drainable heat ratio between Nb_3Sn and Nb-Ti with poorly permeable insulation (SSC type) is almost four (Q column). Such a ratio, in agreement with that reported in previous works [26], is due to the higher temperature margin available to Nb_3Sn, shown in the ΔT column, and to the higher bulk thermal conductiv-

TABLE IV. Maximum drainable heat from Nb-Ti and Nb_3Sn coils.

SC technology	Note		B [T]	J_{ov} [A/mm^2]	J [A/mm^2]	J/Jc	ΔT [K]	Q [mW/cm^2]
Nb-Ti	Insulation	SSC	9	781	1952	0.85	0.58	7
		LHC						10
		ENH						108
Nb_3Sn	Operating conditions	As Nb-Ti			1562	0.25	7.53	203
		Specific	13.5	1218	2436	0.85	1.52	26

ity of epoxy + fiber glass with respect to polyimide, shown in Fig. 5.

However, Nb_3Sn can be exploited to have a high critical temperature sacrificing the available current density, as shown in the 4th row of Table IV. In such a case, we feed Nb_3Sn coil with the same overall current density as Nb-Ti (J_{ov} column) so that, on one hand, the overall current density of Nb_3Sn is only 25% (J/J_c column) of its specific critical value, on the other hand, the available temperature margin (ΔT column) is around 15 times greater than the one available to Nb-Ti. The resulting heat (Q column) drainable from Nb_3Sn is 20 times the one of Nb-Ti.

In Nb_3Sn, the maximum heat transfer is directly related to the available temperature margin because heat can be evacuated only through solid conduction. Therefore increasing heat transfer in Nb_3Sn means decreasing current density. In Nb-Ti, instead, the excellent thermal conductivity of helium allows disentangling almost completely temperature margin and maximum heat transfer: heat transfer can be greatly increased by enhancing insulation permeability, without sacrificing current density. This occurrence corresponds to the third row of Table IV where, thanks to the enhanced insulation detailed in Sec. V, the maximum heat transfer of Nb-Ti is increased by a factor of 10 with respect to the one achievable with state-of-the-art (LHC) insulation.

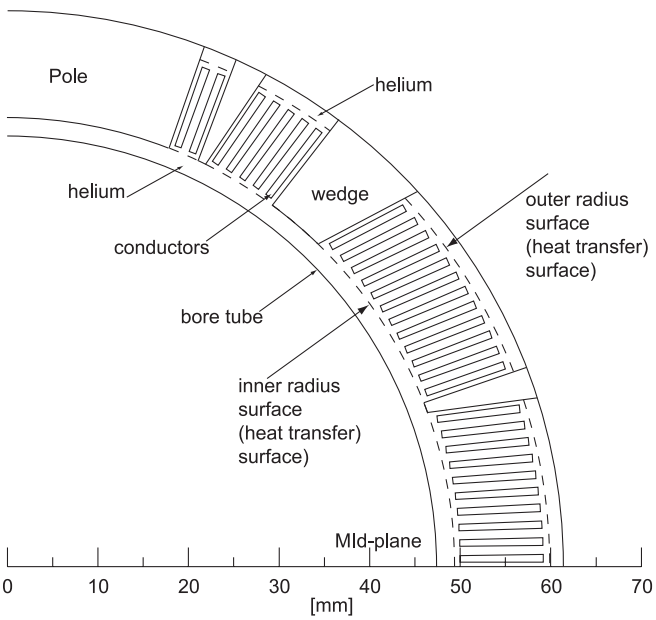

FIG. 15. Transverse cross section of cosθ coil (one quarter).

VIII. CONCLUSIONS

Nb-Ti cables can be wrapped with a nonsealed insulation, providing thus a good heat transfer to superfluid helium until helium is locally saturated. Mechanical, electrical, and thermal properties of the presented enhanced insulation have to be experimentally confirmed.

On the other hand, Nb_3Sn can profit of a higher temperature margin to reach a good heat transfer rate in spite of its typically helium-tight insulation.

We have quantified the expected differences of the two technologies with respect to heat transfer from cable to superfluid helium in several conditions. The relevant analysis shows that when considering state-of-the-art insulation schemes there is, in terms of maximum drainable heat at a given operating condition, a clear advantage of using Nb_3Sn instead of Nb-Ti.

However, theoretically, there is a large margin of improvement of state-of-the-art insulation schemes for Nb-Ti cables in terms of heat transfer potential.

If our first experimental results will be confirmed by direct measurements of temperature rise in the upcoming heat transfer tests, in superfluid helium there would be no advantage in using Nb_3Sn in place of Nb-Ti in terms of heat extraction from the cable.

[1] *LHC Design Report*, edited by Brüning Oliver *et al.* (CERN, Genève, 2004), Vol. 1.
[2] R. Bossert *et al.*, IEEE Trans. Appl. Supercond. **7**, 751 (1997).
[3] L. Tkachenko *et al.*, EPAC 2004, 9th European Particle Accelerator Conference, Lucerne, Switzerland, 2004, pp. 1750–1753.
[4] J. Billan, International Symposium on High Voltage Insulation for Low Temperature Application, Wroclaw, 1976; also in Report no. CERN-ISR-LTD-76-15.
[5] T. S. Jaffrey *et al.*, PAC 93, Particle Accelerator Conference, Washington, DC, 1993, p. 2769.
[6] C. H. Dustmann, M. Forster, and D. Bonmann, IEEE Trans. Magn. **24**, 1338 (1988).
[7] M. Anerella *et al.*, PAC 93, Particle Accelerator Conference, Washington, DC, 1993, p. 2790.

[8] D. Evans and J. T. Morgan, *Advances in Cryogenic Engineering (Materials)*, edited by F. R. Fickett and R. P. Reed (Plenum Press, New York, 1992), Vol. 38, p. 413.
[9] A. Devred, IEEE Trans. Appl. Supercond. **12**, 1232 (2002).
[10] A. den Ouden *et al.*, Adv. Cryog. Eng. **38**, 635 (1992).
[11] J. A. Rice, P. E. Fabian, and C. S. Hazelton, IEEE Trans. Appl. Supercond. **9**, 220 (1999).
[12] A. Puigsegur, L. Quettier, J. Rey, F. Rondeaux, and E. Prouzet, IEEE Trans. Appl. Supercond. **16**, 1769 (2006).
[13] D. S. Matsumoto, C. L. Reynolds, Jr., and A. C. Anderson, Phys. Rev. B **16**, 3303 (1977).
[14] V. Arp, Cryogenics **10**, 96 (1970).
[15] S. W. Van Sciver, *Helium Cryogenics* (Plenum Press, New York, 1986).
[16] N. Kimura *et al.*, Cryogenic Engineering Conference, Portland, OR, 1997.
[17] C. Meuris, B. Baudouy, D. Leroy, and B. Szeless, Cryogenics **39**, 921 (1999).
[18] J. Lawrence, A. B. Paterl, and J. G. Brisson, Cryogenics **40**, 203 (2000).
[19] L. Imbasciati *et al.*, IEEE Trans. Appl. Supercond. **13**, 1788 (2003).
[20] A. Kashani and S. W. Sciver, Cryogenics **25**, 238 (1985).
[21] B. Baudouy, Cryogenics **43**, 667 (2003).
[22] E. Todesco and J.-P. Koutchouk, LHC LUMI 06, Valencia, Spain, 2006.
[23] B. Baudouy, M. X. François, F.-P. Juster, and C. Meuris, Cryogenics **40**, 127 (2000).
[24] L. Chiesa *et al.*, IEEE Trans. Appl. Supercond. **11**, 1625 (2001).
[25] J. Gorter and J. H. Mellink, Physica (Amsterdam) **15**, 285 (1949).
[26] A. Zlobin *et al.*, EPAC 2002, European Particle Accelerator Conference, Paris, France, 2002.